

Modeling of the CVD Deposition Process for Parylene-C to Predict Thin Film Growth

Kevin Baca

Department of Physics and Astronomy, University of New Mexico, Albuquerque, NM 87106, USA

Advisor: Steven Larson

Advanced Thin Films & Processing Group, Sandia National Laboratories, Albuquerque, NM 87123, USA

(Dated: May 2, 2024)

Abstract— A fluid simulation is developed to model the chemical vapor deposition of Parylene thin films in a real deposition system with the hope accurately of predicting the uniformity of film growth throughout the chamber. This model makes use of the most current reference correlations for the various fluid properties of the gaseous monomer para-xylylene, as well as including some models for boundary conditions that occur near walls due to interactions with solid surfaces. Additionally, existing models for the kinetic processes that occur near surface boundaries are also investigated and experimentally verified. In doing so, a more general expression for the deposition rate of Parylene is considered that incorporates arbitrary powers of pressure, m , termed the order of the reaction. Results obtained from thin channel measurements and thickness profile measurements give conflicting values of m and inconsistencies with existing models, revealing that the exact kinematics of the adsorption of para-xylylene is still poorly understood. However, bulk flow properties do seem to be accurately modeled by the simulation, predicting many key features of the final flow. Using the results from our simulation, a value of $m = 2.0847$ is reported, giving an average error of only 0.3276% in the film thickness profile. These results open the pathway towards the application of similar algorithms in the future for use in predicting film uniformity in other industrial and commercial processes, as well as introducing further areas of refinement that could bring results closer to reality.

INTRODUCTION

Poly-para-xylylenes (Parylene) are a class of polymers that have found a rich abundance of applications both in industry and research applications. Along with many desirable material properties such as biocompatibility, a high dielectric constant, and water and chemical resistant properties, the main feature that drives the use Parylene is its ability to be conformally coated with relative ease in a thin-film deposition process known as chemical vapor deposition (CVD). Because of this, Parylene films have found a wide variety of applications in MEMs, biomedical, micro-electronics, and industrial processes, making it increasingly important to study the properties of this material and how it is deposited [1].

The method by which Parylene is deposited generally involves the use of the free-radical monomer, para-xylylene (p-xylylene), which is introduced from the vapor phase to a solid substrate surface. From here it can adsorb onto the surface of the material and react with the tail ends of polymer chains of the already deposited Parylene in a self-perpetuating reaction. This process was first discovered by M. Szwarc in 1947 who managed to produce the monomer via the pyrolysis of a mixture of toluene and various xylenes to produce a thin film [2][3]. The process has since been streamlined thanks to the work of William Gorham who, in 1966, discovered a

more direct route to Parylene deposition via the pyrolysis of the dimer di-para-xylylene [4]. He found that at sufficiently low pressures and high enough temperatures, the dimer could be pyrolyzed into its monomer form in a process known as "cracking". This method is generally preferred for its improved purity and film uniformity, and makes up the majority of commercial and industrial applications today.

The following four-step process is commonly used to deposit Parylene films: **1)** the solid dimer is sublimated at temperatures of about 130 °C, **2)** the gas is pyrolyzed at temperatures in excess of 550 °C, **3)** the monomer is transported to the room temperature substrate, and **4)** the monomer adsorbs onto the surface of the material and reacts to grow a polymer film.

The uniformity of thin films produced in this has long been an area concern for Parylene depositions and CVD processes as a whole. Higher uniformity coatings would allow for more consistent film properties to be guaranteed, which would greatly increase the application space of this material. A variety of approaches have been attempted to improve uniformity of Parylene films, including the use of an inert carrier gas and the introduction of a planetary system, as has been attempted by our group [1][5]. However, in order to better predict factors such as film uniformity and the consistency of film thicknesses, a proper model describing the entire deposition process

must be considered. It is for this reason that the task was taken to compile some of the most current and accurate models involving the deposition of Parylene and apply these in a dynamics simulation to accurately predict film growth in a deposition system. Results could then be empirically validated by measuring uniformities obtained in the real system. Once an accurate simulation is established, the hope is that results can be applied towards future simulations in order to better optimize film uniformity in current and future systems.

A final note is that, in addition to the regular variant of Poly-para-xylylene (Parylene-N) discussed so far, there exist a variety of other types of Parylene used for different applications. Among others, these variants include Parylene-C, Parylene-D, and Parylene-F. The main difference between these molecules lies in the substitution of one or more of the hydrogen atoms on the benzene ring that typically makes up the backbone of Parylene-N for other functional groups. All these variants have slightly different chemical, electrical, and physical properties that are important to consider. For the purposes of this study, we will be focusing our attention on Parylene-C, although the methods used here should be generally applicable to all variants of Parylene.

MATERIALS & METHODS

Adsorption Model for the Deposition of PPX

The exact mechanisms of the surface chemical reactions for Parylene depositions are still not yet fully understood, especially at lower pressures near the known cutoff point at which deposition does not occur. A unique feature of Parylene deposition compared to other CVD processes is that the deposition rate decreases with temperature and increases with partial pressure of the monomer [3]. This leads to the conclusion that deposition is primarily dominated by surface coverage and not the kinetics of the chemical reactions that lead to polymerization. Based on this, Fortin *et al.* proposes a simple model involving a two-step process of physisorption and chemisorption at the surface [3]. In this model, the initial physisorption step is treated using Langmuir-type adsorption at the surface [6]. In such a model, molecules are free to adsorb and desorb onto the surface at a limited number of reactive sites in a reversible, isothermic process. The second chemisorption step involves the polymerization of the monomer and subsequent growth of the film.

The final rate of adsorption is related to the probability that a single collision of a gas molecule will result in a deposition. This fraction is denoted S and is commonly known as the "sticking coefficient" of the gas. Its value depends on the energetics of the reaction at the surface sites and is typically dependent on the temperature

of the surface. The sticking coefficient for p-xylylene is low, generally on the order of between 1,000 and 10,000 [7]. In many cases this is ideal as it allows p-xylylene to penetrate deep in to crevasses to coat high aspect ratios features at the cost of a slower deposition process, so any sufficient model will need to capture this effect.

Expressed in terms of the sticking coefficient, the film's growth rate is then evidently given by,

$$R = N_A V_m S W$$

where W is the number of collisions per second, given by $W = p/(2\pi mkT)$, N_A is Avogadro's number, V_m is the molecular volume of a single molecule, m is the mass of a molecule, k is Boltzmann's constant, and T is the temperature of the gas [8]. This gives the formula for the deposition rate as

$$R_d = \frac{N_A V_m S p}{2\pi mkT} \quad (1)$$

Because physisorption typically has a negligible activation energy, Fortin *et al.* assumes that the physisorption step occurs freely and proposes that chemisorption acts as the rate-limiting step for this reaction. Thus, the expression for the sticking coefficient is determined fully by the kinetics of the chemisorption step. From there, he derives an expression for the sticking coefficient in the steady-state conditions based on the activation energy in the chemisorption step. This is given in terms of,

$$S = S_0(1 - \theta) = \frac{(1 - \theta)}{1 + V e^{-\Delta E/kT_s}} \quad (2)$$

where ΔE is the difference in energies of the physisorption and chemisorption wells given by a Lennard-Jones potential, V is the pre-exponential constant, T_s temperature of the substrate, and θ coverage of the surface, which represents the fractional number of reaction sites that are occupied. The paper also assumed that physisorption may occur at all sites on the surface, regardless of occupancy, so that the coverage only depends on the fraction of available chemisorption sites. Importantly, for this model the conditions being considered are taken to be at steady state so that $(1 - \theta)$ may be taken to be constant during the reaction. Also, because the number of reactive sites is related to the polymer chain length, $(1 - \theta)$ is taken to be fairly constant over the range of pressures and temperatures being considered [3]. Based on kinetic arguments, the growth rate of Parylene is expected to scale with the square of pressure for volume-phase reactions and linearly with pressure for surface reactions [9][5]. However, a much more complicated dependence is actually empirically observed. Other deposition rate equations have been proposed, all involving the kinetics of the polymerization reaction and resulting in differing powers of p in the final expression [5][10]. For example, among the first of these comes from Beach [11], who considers the kinetics in terms of an initiation reaction and

subsequent propagation reactions that occurs. The initiation reaction results in the production of a new polymer chain, involving the consumption of an unknown number of monomer units λ , denoting the order of the reaction. From this, two propagation centers are created at the ends of the polymer chain whereby propagation reactions may occur and further grow the film. By relating the concentration of the monomer near the growth surface to pressure and considering bulk-phase reactions within the gas, Beach is then able to give an expression for the growth rate of the film that is proportional to $p^{(\lambda+3)/4}$.

Nonetheless, these additional models are still worth investigating due the relative obscurity of Parylene reactions at the low pressures and temperatures used in a typical CVD process. Because of this, in addition to Fortin's chemisorption model which scales linearly with p , a model based on arbitrary reaction orders p^m is also investigated as is suggested by Beach's and other proposed models.

Thin Channel Model

In order to investigate the kinetics reaction occurring at the surface of our substrates, a similar experiment to that carried out by Ramachandran et. al. was performed. In this experiment, deposition is carried out in a long, thin, rectangular channel with a height on the order of a few microns. With these dimensions the Knudsen-number, defined as

$$Kn = \frac{\lambda}{L} \quad (3)$$

where λ is the mean free path of the gas, and L is the characteristic length of the problem, is small enough that convective terms of the Navier-Stokes equations can be neglected, and a simple diffusion model can be adopted. The model can be further simplified by assuming that the width of the gap is large enough to consider this a 2-dimensional problem. Because the temperatures during the reaction are assumed to be fairly constant, Ramachandran et. al. adopts a generalized deposition rate equation of

$$R = R_D c^m \quad (4)$$

where c is the concentration of gas at the surface, m is the presumed order of the reaction, and R_D is a proportionality coefficient assumed to be constant over the course of the deposition. This equation is valid assuming that the concentration in the gap is directly proportional to the pressure. Since the pressures considered in this experiment should be on the order of 10 mTorr, the ideal gas law should well approximate the equation of state for our gas so that this assumption holds.

By considering Fick's Diffusion Law and mass continuity, the authors are then able to derive a diffusion equation. This, along with the rate of deposition, creates a system of PDE that models the film growth in the gap. Put in dimensionless form, the problem becomes

$$\frac{\partial}{\partial \bar{t}} \bar{h}(\bar{t}, \bar{x}) = -\bar{c}^m(\bar{t}, \bar{x}) \quad (5)$$

$$\frac{\partial}{\partial \bar{x}} \left(\bar{h} \frac{\partial}{\partial \bar{x}} \bar{c} \right) = B \bar{c}^m \quad (6)$$

where the variables $\bar{t} = \frac{R_D C^m}{H} t$, $\bar{x} = \frac{x}{L}$, $\bar{h} = \frac{h}{H}$, and $\bar{c} = \frac{c}{C}$ are dimensionless variables related to the time t , distance along the gap x , half the height in the gap $h(x, t)$, and the concentration $c(x, t)$ respectively. The constants used are the length of the gap L , half the initial height of the gap H , the time of the deposition τ , and the average concentration $C = \left(\frac{1}{\tau} \int_0^\tau c_0^m(t) dt \right)^{1/m}$ defined such that the total height deposited at the entrance of the gap is given by

$$\bar{H} = \tau R_D C^m \quad (7)$$

$c_0(t)$ is concentration outside the gap which defines the boundary condition for c ,

$$c(t, 0) = c_0(t)$$

This along with the no-flux boundary condition at the end of the channel and our initial conditions complete the PDE,

$$\frac{\partial c}{\partial x}(t, L) = 0, \quad c(0, x) = 0, \quad h(0, x) = H$$

The resulting domain of the problem is $[0, 1]$ for \bar{x} and $[0, \frac{\tau R_D C^m}{H}]$ for \bar{t} , with $\frac{\tau R_D C^m}{H} = \frac{\bar{H}}{H}$ from equation (7).

We finally see that non-dimensionalization has reduced the system to that of one having a two free parameters B and $\frac{\bar{H}}{H}$. The constant B is given by

$$B = \frac{\rho L^2 R_D C^{m-1}}{MHD}$$

where D is the diffusion coefficient of the gas, $\rho = 1177 \text{ kg/m}^3$ is the density of the Parylene film based on the density of the common α crystal structure of Parylene present at temperatures above $-17 \text{ }^\circ\text{C}$ [1], and $M = 2.2981861 \times 10^{-25} \text{ kg}$ is the mass of a single p-xylylene molecule. D can be estimated as $D = \frac{3\pi\lambda\nu}{16}$, where $\lambda = \frac{k_B T}{\sqrt{2}\sigma P}$ is taken to be the mean free path of the gas, $\sigma = 4.2 \times 10^{-19} \text{ m}^2$ is taken to be the average cross-sectional area of the molecule, P is the average pressure during the deposition, and $\nu = \sqrt{\frac{8kT}{\pi m}}$. Thus, B can finally be expressed as

$$B = \frac{8L^2 \bar{H} \rho \sigma}{3\tau H} \sqrt{\frac{1}{\pi M k T}} \quad (8)$$

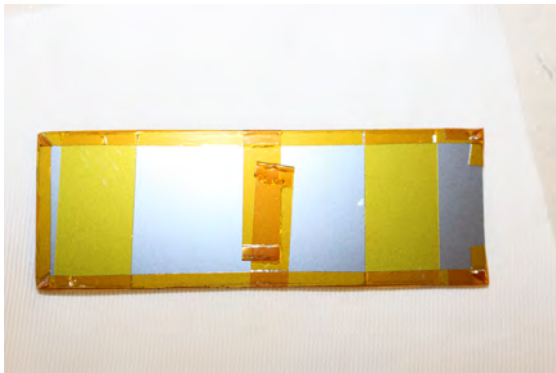


FIG. 1: Silicon plates coated with Parylene-C and sealed together with Kapton tape to form the channels used in the thin channel experiment.

Thin Channel Experiment

To prepare the thin channels used for this experiment, two silicon wafers were first cut into rectangles with dimensions of 75.75 mm by 25.00 mm. To form the channel, Kapton tape of width 13mm was put along the length of each wafer. An initial coating of Parylene was then deposited onto the wafers to form the gap height. This height was measured using white-light interferometer to obtain a value of $H = 43.52 \mu\text{m}$. The film was then carefully cut from around the tape and the tape removed, creating the desired gap. The two wafers were then sandwiched together and the edges around the perimeter were sealed using Kapton tape everywhere except for one of the gap entrances. A picture of the channel used is shown in figure 1. A final deposition was then carried out on newly formed channel to a height of $8 \mu\text{m}$. A Pirani pressure gauge in the deposition system allowed for the pressure to be monitored and logged during the deposition process, which could then be used to account for the concentration initial condition via the ideal gas law $c_0(t) = p(t)/kT$. The final deposition height was recorded using a flat silicon witness placed near the entrance of channel. The value \bar{H} was then recorded by measuring the film thickness on this witness with a white-light interferometer.

Slip Flow Considerations

The Navier-Stokes-Fourier (N-S-F) equations are a set of three non-linear partial differential equations that are meant to fully describe the dynamics of a given fluid [12]. The first of these equations is called the continuity equation and can be written as

$$\frac{\partial \rho}{\partial t} + \nabla \cdot (\rho \mathbf{u}) = 0 \quad (9)$$

where ρ is the fluid density and \mathbf{u} is the fluid's velocity.

The momentum equation is given by

$$\frac{\partial}{\partial t}(\rho \mathbf{u}) + \nabla \cdot (\rho \mathbf{u} \otimes \mathbf{u}) + \nabla p = \nabla \cdot S \quad (10)$$

where p is the pressure and S is the viscous stress tensor of the fluid.

Finally, the energy equation is given by

$$\frac{\partial}{\partial t}(\rho E) + \nabla \cdot (\rho E \mathbf{u}) + \nabla q + \nabla \cdot (p \mathbf{u}) = \nabla \cdot (S \mathbf{u}) \quad (11)$$

where $\rho E = \rho e + \frac{\rho |\mathbf{u}|^2}{2}$ is the total energy, e is the internal energy, and q is the heat flux.

Generally, these equations only apply in the continuum regime, as they are derived by averaging the Boltzmann equations and assuming a Maxwell-Boltzmann distribution. However, due to the low pressures involved during depositions, the possibility of more rarefied flows needs to be considered.

It has been well known for over a century that N-S-F equations struggle to predict rarefied flows. To remedy this, in 1879 James Clark Maxwell first proposed a set of boundary conditions that would allow for the continued use of the Navier-Stokes equations within these regimes [13][14]. He did this by accounting for some fraction σ_u of the molecules are reflected diffusely, while the rest are reflected specularly. This resulted in a modified boundary condition where the fluid partially "slipped" along the surface of walls. The regime for which this boundary condition occurs is for moderately low values of the Knudsen number and is fittingly called the slip flow regime. The boundary condition describing this flow is given by the equation

$$\mathbf{u} - \mathbf{u}_w = \frac{2 - \sigma_u}{\sigma_u} Kn \left(\frac{\partial \mathbf{u}}{\partial n} \right)_w$$

where \mathbf{u}_w is the velocity of the wall, and $\left(\frac{\partial}{\partial n} \right)_w$ is the spacial derivative normal to the wall.

The fraction σ_u is now known as the tangential momentum accommodation coefficient on the account that other accommodation coefficients have been discovered. Maxwell's original boundary conditions have also since been modified to account for additional effects including wall curvature and thermal creep. This new expression is given by the following boundary condition

$$\mathbf{u} - \mathbf{u}_w = \frac{2 - \sigma_u}{\sigma_u} \lambda \left(\frac{\partial \mathbf{u}}{\partial n} + \frac{\partial \mathbf{v}}{\partial t} \right) + \frac{3}{4} \frac{\mu R}{p} \frac{\partial T}{\partial t} \quad (12)$$

where \mathbf{v} is the normal component of the velocity to the wall, μ is the viscosity, and R is the specific gas constant in units of J/kg/K [15].

A phenomenon known as "temperature jump" is also observed in this regime whereby the temperature of the gas near the wall differs from the temperature of the wall in a rapid "jump". This boundary condition is given by,

$$T - T_w = \frac{2 - \sigma_T}{\sigma_T} \frac{2\gamma}{\gamma + 1} \frac{\lambda}{Pr} \frac{\partial T}{\partial n} \quad (13)$$

where σ_T is the thermal accommodation coefficient which indicates the fraction of energy exchanged to the surface, γ is the specific heat ratio for the gas, $Pr = \frac{c_p \mu}{K}$ is the Prandtl number of the flow, c_p is the gas's specific heat, and K is the thermal conductivity of the gas. This boundary condition is known as the Smoluchowski jump boundary condition after its discoverer.

In addition to this, adsorption of gas needs to be accounted for in our boundary conditions. Mirroring the considerations from Fortin *et al.* it was considered reasonable to treat these boundary conditions based on a Langmuir adsorption isotherm [3]. Le *et al.* derives a modification to the Maxwell slip and Smoluchowski jump boundary conditions based on this model [16]. In addition to the typical assumptions of a Langmuir adsorption isotherm, this model also assumes that the accommodation coefficients of the gas are close to 1, as is typically the case for most flows. The new boundary conditions are then solely based on the fractional coverage of the surface θ as introduced earlier. These boundary conditions are given by

$$\mathbf{u} - \mathbf{u}_w = \frac{\lambda}{\theta} \left(\frac{\partial \mathbf{u}}{\partial n} + \frac{\partial \mathbf{v}}{\partial t} \right) + \frac{3}{4} \frac{\mu R}{p} \frac{\partial T}{\partial t} \quad (14)$$

and

$$T - T_w = \frac{\lambda}{\theta} \frac{2\gamma}{\gamma + 1} \frac{1}{Pr} \frac{\partial T}{\partial n} \quad (15)$$

Fluid Properties

Because of the importance of Parylene film growth in many industrial and commercial applications, the properties of p-xylylene have been studied in great detail. In particular, a variety of studies have been carried out to correlate existing data with current models on various transport and thermophysical properties of the gas. One of the most detailed of these models comes from Zhou *et al.* who used group contribution methods to compile equation of state data from papers dating as far back as the late 19th century. This was then used to fit an expression for the Helmholtz free energy of p-xylylene [17]. The function is expressed in dimensionless form and broken up into ideal and residual components as

$$\frac{a(\rho, T)}{RT} = \alpha(\delta, \tau) = \alpha^0(\delta, \tau) + \alpha^r(\delta, \tau) \quad (16)$$

where a is the Helmholtz free energy per unit mole, R is the ideal gas constant in units of $\text{J}(\text{mol}\cdot\text{K})^{-1}$, α^0 is the dimensionless ideal-gas energy contribution, and α^r is the residual contribution. The other dimensionless variables are given by $\delta = \rho/\rho_c$ and $\tau = T_c/T$, which are expressed in terms of the critical point values for p-xylylene, ρ_c , T_c , and p_c . α^0 was fitted using ideal-gas heat capacity data

in the form of the expression

$$\alpha^0 = \ln \delta + (\nu_0 - 1) \ln \tau + a_1 + a_2 \tau + \sum_{i=1}^{I_{ideal}} \nu_i \ln \left[1 - \exp \left(\frac{-u_i \tau}{T_c} \right) \right] \quad (17)$$

where a_1 , a_2 , ν_i , and u_i are constants used in the fit.

The functional form of the residual contribution is based on empirical models and was fitted using various properties such as vapor pressure, saturation densities, and other equation of state data. This function is expressed as

$$\alpha^r = \sum_{i=1}^{I_{Pol}} n_i \delta^{d_i} \tau^{t_i} + \sum_{i=I_{Pol}+1}^{I_{Pol}+I_{Exp}} n_i \delta^{d_i} \tau^{t_i} \exp(-\delta^{l_i}) + \sum_{i=I_{Pol}+I_{Exp}+1}^{I_{Pol}+I_{Exp}+I_{GBS}} n_i \delta^{d_i} \tau^{t_i} \exp(-\eta_i(\delta - \epsilon_i)^2 - \beta_i(\tau - \gamma_i)^2) \quad (18)$$

where n_i , d_i , t_i , l_i , η_i , ϵ_i , β_i , and γ_i are all fitting constants. The exact values of all constants used can be found in Zhou *et al.*

With this expression for the Helmholtz free energy, most relevant fluid properties can be derived through its various derivatives [18]. For example, the equation of state is given by $p = \rho^2 \left(\frac{\partial a}{\partial \rho} \right)_T$, entropy per mole is given by $s = - \left(\frac{\partial a}{\partial \tau} \right)_\rho$, and internal energy per unit mole is given by $u = a + Ts$. In similar ways, the constant volume and pressure heat capacities, c_v and c_p , entropy h , and the compressibility factor Z can also be derived. Using the above expression, the equation of state can be explicitly calculated as,

$$p(\tau, \delta) = \rho R_r T + \rho R_r T \left[\sum_{i=1}^{I_{Pol}} n_i d_i \delta^{d_i} \tau^{t_i} + \sum_{i=I_{Pol}+1}^{I_{Pol}+I_{Exp}} n_i (d_i - l_i \delta^{l_i}) \delta^{d_i} \tau^{t_i} \exp(-\delta^{l_i}) + \sum_{i=I_{Pol}+I_{Exp}+1}^{I_{Pol}+I_{Exp}+I_{GBS}} n_i (d_i - 2\eta_i \delta(\delta - \epsilon_i)) \delta^{d_i} \tau^{t_i} \times \exp(-\eta_i(\delta - \epsilon_i)^2 - \beta_i(\tau - \gamma_i)^2) \right] \quad (19)$$

$$+ \sum_{i=I_{Pol}+1}^{I_{Pol}+I_{Exp}} n_i (d_i - l_i \delta^{l_i}) \delta^{d_i} \tau^{t_i} \exp(-\delta^{l_i}) \quad (20)$$

$$+ \sum_{i=I_{Pol}+I_{Exp}+1}^{I_{Pol}+I_{Exp}+I_{GBS}} n_i (d_i - 2\eta_i \delta(\delta - \epsilon_i)) \delta^{d_i} \tau^{t_i} \quad (21)$$

$$\times \exp(-\eta_i(\delta - \epsilon_i)^2 - \beta_i(\tau - \gamma_i)^2) \quad (22)$$

The range of validity for these equations is stated to be in temperature ranges of 286.4 K to 700 K and pressures of up to 200 MPa, well within the ranges used in this simulation.

The remaining properties of the gas were found using similar correlation studies. Using the original model by Zhou *et al.*, the authors of Mylona *et al.* further develop reference correlations for the thermal conductivity

of p-xylylene [19]. Their original model accounts for the critical enhancement of the monomer during crossover, which is omitted here due to the low pressures present in the problem being considered. The model for the thermal conductivity λ can then be expressed in terms of dilute-gas limit $\lambda_0(T)$ and residual contributions $\Delta\lambda(\rho, T)$ as

$$\lambda = \lambda_0(T) + \lambda_0(\rho, T)$$

The functional forms of the diffuse limit can be expressed as

$$\lambda_0(T) = 0.0541409 \frac{(C_p^0/k)\sqrt{T}}{S_\lambda} \quad (23)$$

where C_p^0 is the ideal heat capacity derived from Zhou *et al.* and S_λ is an effective generalized cross section of the gas that was fit to the form $S_\lambda = b_0 + b_1/T$ for arbitrary coefficients b_0 and b_1 .

The residual contribution can be expressed as

$$\Delta\lambda(\rho, T) = \sum_{i=1}^5 (B_{1,i} + B_{2,i}(T/T_c))(\rho/\rho_c)^i \quad (24)$$

where $B_{1,i}$ and $B_{2,i}$ are coefficients used in the fit. Again, values of these constants can be obtained from the original paper by Mylona *et al* [19]. The validity of these equations is stated to be accurate from the triple point of p-xylylene (286 K) up to 700 K.

Finally, reference correlations of the viscosity of p-xylylene are obtained from Balogun *et al* [20]. The model used accounts for four viscosity contributions $\eta_0(T)$, $\eta_1(T)$, $\Delta\eta(\rho, T)$, and $\Delta\eta_c(\rho, T)$ corresponding to the zero-density limit, the initial linear density dependence, the critical enhancement of the gas near the critical point, and the residual viscosity. As before, critical contributions are neglected in this study. The final form of the viscosity η is then given by

$$\eta(\rho, T) = \eta_0(T) + \eta_1(T)\rho + \Delta\eta(\rho, T)$$

The zero-limit viscosity for p-xylylene is expressed as

$$\eta_0(T) = 0.22005 \frac{\sqrt{T}}{S_\eta} \quad (25)$$

where S_η is the effective collision cross section of the monomer units of in nm^2 . This is fit to the form $\ln(S_\eta) = A_0 + \frac{B_0}{T} + \frac{C_0}{T^2}$ for arbitrary coefficients A_0 , B_0 , and C_0 . The initial density dependence term is also fit to this form

$$\eta_1(T) = A_1 + \frac{B_1}{T} + \frac{C_1}{T^2} \quad (26)$$

for arbitrary coefficients A_1 , B_1 , and C_1 . Lastly, the residual contribution is given in terms of the dimension-

less quantities $\delta = \rho/\rho_c$ and $\tau = T/T_c$ introduced earlier,

$$\Delta\eta(\rho, T) = \delta^{2/3} \sum_{i \in \{1.5, 2, 3, 4, 5, 11\}} D_i \delta^i + \frac{\delta^{2/3}}{\sqrt{\tau}} \sum_{i \in \{1.5, 11, 15\}} E_i \delta^i \quad (27)$$

where D_i and E_i are arbitrary fitting coefficients. The range of validity for these equations is stated to be from 286.4-673 K and pressures up to 100 MPa. Values of the fitting constants for p-xylylene can be found in the original paper [20].

These three reference correlations allow for a holistic consideration of all the relevant thermophysical and transport properties of p-xylylene gas over a wide range of pressures and temperatures. With this, the fluid properties of the gas can be fully accounted for within a range of potential simulation conditions while still maintaining a high degree of accuracy.

Fluid Simulation

A diagram of the deposition system used is shown in figure 2. Notable features of the chamber include a horizontal distribution tube (shown to the left of figure 3) used to feed gas into the chamber, a planetary system allowing for parts to be rotated throughout the system, an outlet opposite the distribution tube, and a Pirani gauge present near the back of the chamber. The process involves the sublimation of the dimer di-para-xylylene in a vaporizer chamber where it then passes through the pyrolysis tube which cracks the dimer into its monomer form. The monomer then passes through the deposition chamber where it is allowed to deposit onto room temperature surfaces. Any undeposited gas passes through an outlet into a long, cryogenically cooled cold trap, known as a "cold finger", which absorbs the remaining dimer before it is able to enter the vacuum pump that drives the flow in the system. The cold finger mentioned above is able to reach temperatures as low as tens of kelvin, however, it is sufficiently far enough away from the deposition chamber so as not to significantly impact its temperatures.

In addition to this, the bell jar that forms the main deposition chamber has been retrofitted with an in-situ white-light interferometer to allow for monitoring of the deposited film thickness via a witness placed at the center of the planetary system. This allows for more precise control over the final film's thickness. To create a steady pressure throughout the deposition process, a proportional-integral-derivative controller (PID) is used to control the temperature of the vaporizer chamber so that a set pressure is maintained. This allows for the pressure to remain nearly constant during the deposition.

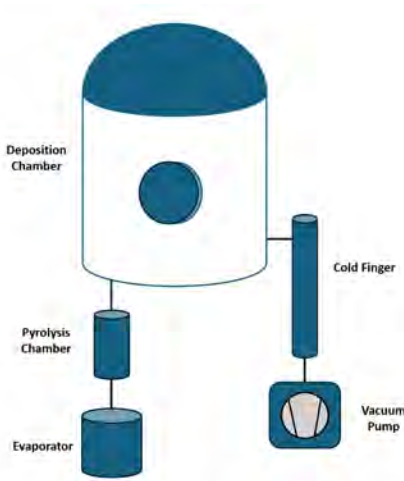


FIG. 2: A diagram showing the various elements of the Parylene deposition system used.

Initial considerations of the Knudsen number $Kn = \lambda/L$ of the gas within the chamber under typical deposition pressures of about 20 mTorr reveal a Knudsen number of approximately 0.02 for the distribution tube and 0.0016 for the main chamber. A Knudsen number in the range of $0.1 < Kn \leq 10$ corresponds the transitional flow regime, $0.001 < Kn \leq 0.1$ corresponds to the slip flow regime, and the continuum flow regime typically requires $Kn \leq 0.001$ [21]. Thus, flow in the distribution tube is in the lower end of the transitional flow regime, while flow in the chamber is firmly within the slip regime. In the transitional regime, slip boundary conditions can still be applied in some cases. Therefore, due to the flow in the distribution tube being on the lower end of this regime, along with the flow in this region of the chamber not being the main area of focus, the slip boundary conditions were also considered reasonable for inside the distribution tube.

The fluid simulation was carried out using the open-source computational fluid dynamics (CFD) simulation software OpenFOAM. The open-source nature of this software allows for a high degree of customization and the implementation of detailed custom codes that wouldn't be possible with other CFD software. This particular simulation was carried out using the rhoCentralFoam solver. This solver is a compressible, density-based solver used to solve the N-S-F equations while explicitly dealing with the viscous stress tensor. These features make it ideal for the implementation of our slip boundary conditions. Because conditions are assumed to reach steady-state in a sufficiently short time interval, only the steady state N-S-F were solved for. A laminar stress model was used for the simulation, accounting for the small Reynolds numbers ($Re = \frac{\rho v L}{\mu}$) estimated for the fluid. In the laminar model diffusion terms such as $\nabla \cdot S$, (10) play a significant role in the solving of the N-S-F equa-

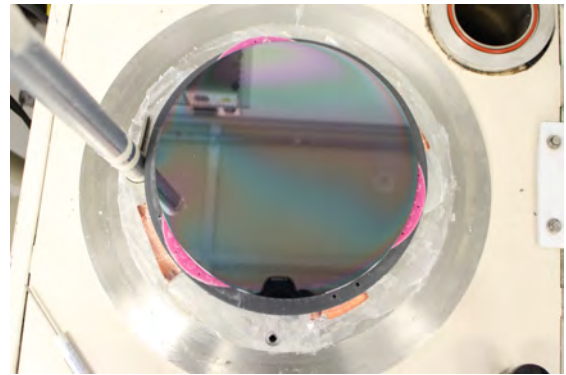


FIG. 3: A top down picture of the 8 in wafer experiment showing the wafer position, the planetary system (center), and the distribution tube (left).

tions compared to the case of turbulent flow.

Due to the low deposition rates of Parylene that occur, the effects of adsorption were considered to have a negligible impact on the main fluid equations. Similarly, although the heat of adsorption of Parylene-C is generally not negligible, and can often be quite large, investigations by Gazicki *et al.* have found that the additional heat from the adsorption of Parylene-C results in the re-evaporation of part of the film in such a way that the net heat exchanged at the surface of a wall is nearly zero [1]. Thus, thermal effects of the film were also considered negligible in affecting the energy equation of the N-S-F equations.

Because of the relative complexity of the geometry of the deposition chamber being considered, a tetrahedral mesh was used to define the domain of the simulation. A cross section of the mesh used is shown in figure 4. The boundary conditions were created by defining a fixed flow rate of gas at the inlet of distribution tube. The outlet flow rate was set based on the inlet flux in order to conserve mass in the system. The inlet mass flow rate was estimated by measuring the change in mass of the dimer, Δm , during the duration, τ , of the deposition. This was done by obtain the average flow rate via the expression

$$\dot{m} = \frac{\Delta m}{\tau}$$

which, of course, assumes that steady-state is reached in fast enough timescales so that this averaged flow rate is nearly equal to the steady-state rate.

The inlet pressure was determined by iteratively adjusting the pressure until the pressure obtained at the position of the pressure gauge closely matched the real steady-state pressure measured. The outlet boundary conditions were set based on free-stream conditions whereby the pressure and temperature gradients are set to zero. The pressure boundary condition at the walls were similarly set to a zero-gradient condition, and the

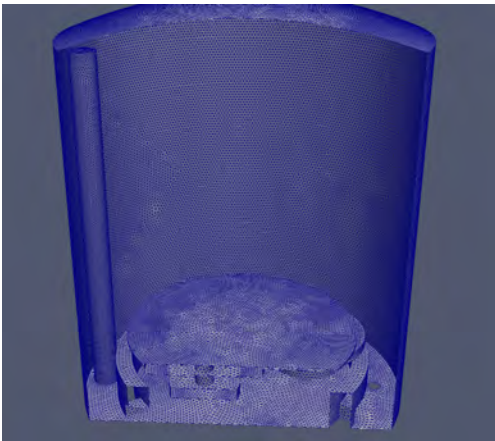


FIG. 4: A cross section showing the surfaces of the mesh used. Here the distribution tube (left), planetary system (center), and outlet (right) can be seen.

temperature was taken to be room temperature at 298 K. Finally, the temperature of the inlet was taken to be close to the pyrolyzation temperature of p-xylene, and was set to 473 K.

DATA & ANALYSIS

Equation of State Saturation Curve

A notable feature of the energy model introduced by Zhou *et al* is its ability to predict phase transitions of the fluid from a liquid to gaseous state. The mechanism behind this is similar to that of the well-studied Van der Waals equation. This is not a coincidence as the proposed model is partially based on higher-order Virial expansions [17]. The result of this is that there exist nonphysical regions of the equation of state plot where the pressure decreases with increasing density. This can be seen in the example isotherm shown in figure 5. Such features were originally studied by Boltzmann in the Van der Waals equations. The model was rectified by noting that regions with $\frac{\partial p}{\partial \rho} \leq 0$ violate the extremum principle of thermodynamics, meaning that no physical states should be observed in these regions [22]. The interpretation of this is that a phase change must occur where a mixture of liquid and gaseous states coexist. The size of this transition zone depends on the temperature being considered, resulting in a saturation curve of the saturation pressures and densities at each temperature. Also, because of the coexistence of gaseous and liquid states, the pressures at the liquid and gaseous density transition points must be equal. Denoting these points as $\rho_{liq}(T)$ and $\rho_{gas}(T)$ respectively, we can express this condition as

$$p(T, \rho_{liq}(T)) = p(T, \rho_{gas}(T)) \equiv p_{sat}(T) \quad (28)$$

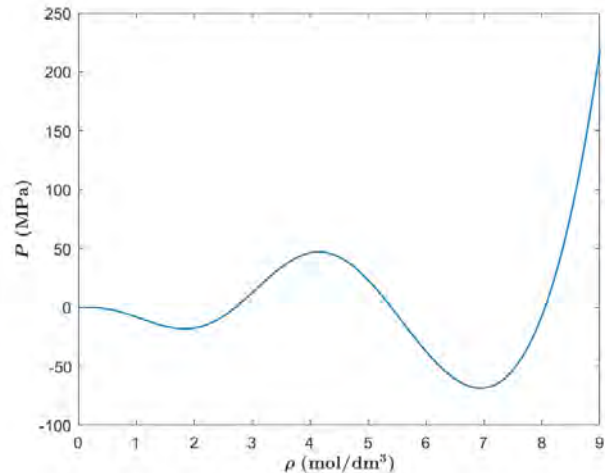


FIG. 5: An example of non-physical behavior from the equation of state isotherm at 300 K

where p_{sat} is defined as the saturation pressure. By providing a second condition that the Gibbs free energy g of the saturated liquid and vapor must be equal,

$$g(T, \rho_{liq}(T)) = g(T, \rho_{gas}(T)) \quad (29)$$

the transition points at a given temperature become fully defined.

Although such phase transitions are not explicitly considered in this model, it becomes important to determine this saturation curve when numerically running the simulation. Because of the way the rhoCentralFoam solver works in OpenFOAM, the transport properties such as heat capacities and the equation of state are expressed as a function of p and T instead of ρ and T . The advantage of this is that unrealistic densities can be avoided. However, this comes at the cost of the equation of state (22) needing to be solved implicitly. For this purpose, Newton's method was employed which requires the use of sufficient initial conditions outside the zone of $\left(\frac{\partial p}{\partial \rho}\right)_T < 0$ where nonphysical solutions are approached. One method of choosing a robust and efficient initial condition is by selecting a value of $\rho_{liq}(T)$ or $\rho_{gas}(T)$ depending on if the given pressure p is below or above the saturation pressure $p_{sat}(T)$. It is for this reason that the task of fitting the saturation curve was taken.

The saturation curve was developed by sampling the saturation pressures and densities at various temperatures on a grid of 10,000 evenly spaced points from 200 K to 616.16 K. These points represent a range slightly below the minimum valid temperature of the equation of state up to the critical temperature of the gas. Saturation values were determined by using Newton's method to find the pressure at which zero Gibbs free energy was attained. Densities at each pressure iteration were deter-

mined by again applying Newton's method to implicitly solve the equation of state. For the initial conditions of these densities, the two spinodal points, given by the condition $\left(\frac{\partial p}{\partial \rho}\right)_T = 0$, were used. These spinodal points were themselves determined using Newton's method with initial conditions determined from an empirical density saturation curve developed by Hales *et al* [23].

Since the Gibbs free energy per unit mole, $g(\rho, T)$ of the fluid could be determined analytically by the relation $g = u + \frac{p}{\rho}M_m - Ts$, where M_m is the molar mass of p-xylylene in units of kg/mol, the difference in Gibbs energy between the two saturation points (29) could be determined analytically without integrating the equation of state. Instead, Newton's method could be employed to solve for the saturation pressure p_{sat} at which $\Delta g = g(T, \rho_{liq}) - g(T, \rho_{gas}) = 0$ by using the derivative $\left(\frac{\partial g}{\partial p}\right)_T = \frac{M_m}{\rho}$ and the mean pressure at the two spinodal points as an initial guess. A single Newton iteration is then given by

$$p_{sat,i+1} = p_{sat,i} - \frac{\rho_{liq,i}\rho_{gas,i}\Delta g}{M_m(\rho_{liq,i} - \rho_{gas,i})}$$

As mentioned earlier, $\rho_{liq,i+1}$ and $\rho_{gas,i+1}$ could then be updated using Newton's method to solve for the two densities at the current pressure. In this way, the saturation pressures and densities were obtained to an accuracy of 1×10^{-6} Pa and 1×10^{-6} kg/m³ respectively.

To allow for efficient computations of saturation values in the main simulation, the obtained values of $\rho_{liq}(T)$, $\rho_{gas}(T)$, and $p_{sat}(T)$ were fit using a cubic spline. The resulting saturation curve is shown in figure 6, and a sample of the corrected equation of state curves at various temperatures is shown in figure 7.

Thin Channel Model Computation

Due to the independence of time and spacial derivative terms in the equations for the thin channel model, the system of equations (5) and (6) were solved using the method of lines [24]. In this approach, the space and time domains were each discretized using $n = 250$ evenly spaced points.

Let $\bar{h}_{i,j} = \bar{h}(i\Delta t, j\Delta x)$ and $\bar{c}_{i,j} = \bar{c}(i\Delta t, j\Delta x)$ denote the indices of these points, where $\Delta x = \frac{1}{n-1}$ and $\Delta t = \frac{H}{H(n-1)}$. \bar{h} is first updated from equation (5) using Euler's method and the previous iteration's values of \bar{c} as given by,

$$\bar{h}_{i+1,j} = \bar{h}_{i,j} - \bar{c}_{i,j}^m \quad (30)$$

The spacial problem (6) can then be solved separately, and is expressed as

$$\frac{\partial \bar{h}_i}{\partial x} \frac{\partial \bar{c}}{\partial x} + \bar{h} \frac{\partial^2 \bar{c}}{\partial x^2} = B\bar{c}^m$$

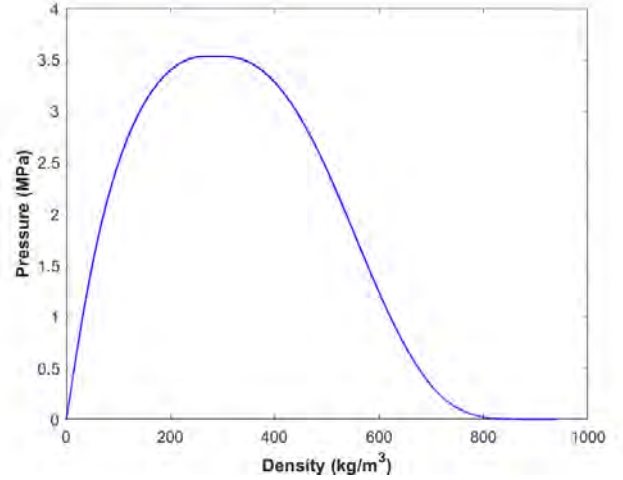


FIG. 6: A plot of the saturation curve fit obtained using cubic splines. This curve is parametrically defined in terms of the temperature T .

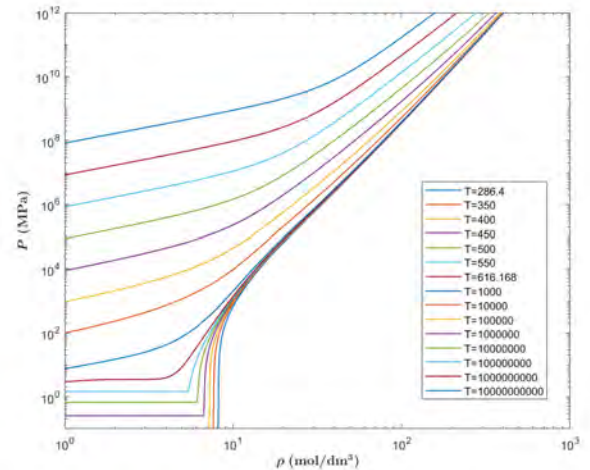


FIG. 7: A plot of various equation of state isotherms accounting for phase transitions below the critical temperature.

A central difference scheme is used to calculate the first order derivative terms, given generally by

$$\frac{\partial y}{\partial x} \approx \frac{y_{i,j+1} - y_{i,j-1}}{2\Delta x}$$

for some variable y . Similarly, the second derivative is approximated using a second-order central differencing scheme given by

$$\frac{\partial^2 y}{\partial x^2} \approx \frac{y_{i,j+1} - 2y_{i,j} + y_{i,j-1}}{\Delta x^2}$$

The resulting discretized system of equations approxi-

mating equation (6) is then given by

$$f(\mathbf{c}^i) = \frac{(\bar{h}_{i,j+1} - \bar{h}_{i,j-1})(\bar{c}_{i,j+1} - \bar{c}_{i,j-1})}{4\Delta x^2} + \bar{h}_{i,j} \frac{\bar{c}_{i,j+1} - 2\bar{c}_{i,j} + \bar{c}_{i,j-1}}{\Delta x^2} - B\bar{c}_{i,j}^m = 0 \quad (31)$$

where the values of \bar{h} are presumed to be known and \mathbf{c}^i is the vector containing the spacial points $\bar{c}_{i,j}$ for $j = 1, \dots, n-2$. The boundary condition $\frac{\partial c}{\partial x}(t, L) = 0$ specifies that $\bar{c}_{i,n-1} = \bar{c}_{i,n-2}$, and the condition $c(t, 0) = c_0(t)$ specifies that $\bar{c}_{i,0} = \frac{c_0(i\Delta t)}{C} \equiv \bar{c}_i^0$.

The Jacobian, $J(\mathbf{c}^i)$, of equation (31) is a tridiagonal matrix with diagonal entries

$$J_{j,j}(\mathbf{c}^i) = -\frac{2\bar{h}_{i,j}}{\Delta x^2} - mB\bar{c}_{i,j}^{m-1}$$

for $j \neq n-2$ and off-diagonal entries

$$J_{j,j+1}(\mathbf{c}^i) = \frac{\bar{h}_{i,j+1} - \bar{h}_{i,j-1}}{4\Delta x^2} + \frac{\bar{h}_{i,j}}{\Delta x^2}$$

and

$$J_{j,j-1}(\mathbf{c}^i) = -\frac{\bar{h}_{i,j+1} - \bar{h}_{i,j-1}}{4\Delta x^2} + \frac{\bar{h}_{i,j}}{\Delta x^2}$$

where the $J(\mathbf{c}^i)$ is an $(n-2) \times (n-2)$ matrix with indices going from 1 to $n-2$. Boundary conditions are accounted for with

$$J_{n-2,n-2}(\mathbf{c}) = \frac{\bar{h}_{i,n-1} - \bar{h}_{i,n-3}}{4\Delta x^2} - \frac{\bar{h}_{i,n-2}}{\Delta x^2} - mB\bar{c}_{i,n-2}^{m-1}$$

Finally, the system can be solved by letting $f(\mathbf{c}^i) = 0$. This can be done iteratively using Newton's method, generalized to multiple dimensions:

$$\mathbf{c}_{k+1}^i = \mathbf{c}_k^i - J(\mathbf{c}_k^i)^{-1} f(\mathbf{c}_k^i) \quad (32)$$

where this equation is evaluated using the Thomas algorithm for tridiagonal systems. This process was repeated until the norm of $f(\mathbf{c}_k^i)$ was less than a tolerance of 10^{-6} . With this, both \mathbf{c}^i and \mathbf{h}^i could be determined at each time step of Euler's method to solve our model.

Comparison of Thin Channel Model with Experimental Results

The resulting film thickness profile predicted by the thin channel model is given by

$$h_f(x) = H(1 - \bar{h}(\tau, \frac{x}{L})) \quad (33)$$

This was compared to experimental measurements obtained via a CompleteEase RC2 ellipsometer (J.A. Woolam). Data was collected over a wavelength range of 200-1000 nm at three different ellipsometry angles of 55° , 65° ,

and 75° . This was done to maximize the range of thickness measurements able to be accurately covered. Measurements were taken along the center of the channel, and a linear map was automatically measured along its length using a built-in translator stage. For this map 25 measurements were taken at a distance of 1 mm apart along the gap, accounting for a total distance of 2.5 cm into the channel. At further distances, thicknesses were found to be too low to be accurately measured. The ellipsometer was also found to struggle with measurements in areas of high thickness gradients, so measurements near entrance of the gap were also not able to be obtained. However, a value for the thickness at the end of the gap could still be estimated by assuming a value equal to the externally measured thickness, as is accounted for in our model.

The general principles of ellipsometry work by obtaining values of the amplitude ratio Ψ and phase differences Δ of light reflecting off a film surface [25]. This data can then be compared to theoretical models given by Fresnel's equations which are parameterized in terms of the thickness and optical constants of the material. This model is then fit to the data by minimizing a certain mean-squared-error estimator that is used to quantify the total error. For these measurements, the mean-squared-error is expressed as

$$MSE = \left(\frac{1}{3n-m} \sum_{i=1}^n \left[\left(\frac{N_{E_i} - N_{G_i}}{0.001} \right)^2 + \left(\frac{C_{E_i} - C_{G_i}}{0.001} \right)^2 + \left(\frac{S_{E_i} - S_{G_i}}{0.001} \right)^2 \right] \right)^{1/2} \quad (34)$$

where n is the number of data points collected, m is the number of fit parameters, the subscript E represents measured data, and the subscript G represents model-generated data. N , C , and S are variables expressed in terms of Ψ and Δ as

$$N = \cos(2\Psi), \quad C = \sin(2\Psi) \cos(\Delta), \\ \text{and } S = \sin(2\Psi) \sin(\Delta)$$

In order to account for the effects of error in this experiment, a weighted average of the thickness measurements taken at each ellipsometry angle is calculated to reduce the effects of low-quality measurements. Thus, the weights were chosen based on the inverse square of the MSE,

$$w_i = (MSE)^{-2}$$

In addition to this, data points with MSE above a certain threshold $MSE > E_{thres}$ were rejected from the data set. This threshold was chosen as $E_{thres} = 100$ which was found to give the results most consistent with theory. A plot of the final data used for comparison with models is shown in figure 9.

Because the exact temperatures of the gas during the reaction weren't fully known, the parameter B from equation (8) was allowed to vary freely. The optimal value of B was obtained by minimizing the residual sum of squares error between the experimental thickness distribution data and the computed model. This was done using the Nelder-Mean simplex algorithm as implemented by the function `fminsearch` in the programming platform MATLAB [26]. From this information, it became possible to derive estimate the temperature of the gas by solving equation (8) for T :

$$T = \frac{N_A}{\pi m k} \left(\frac{8L^2 \bar{H} \rho \sigma}{3\tau H B} \right)^2 \quad (35)$$

Mapping Chamber Thickness Profile

To create a profile of the flow in the deposition chamber, an 8-inch diameter silicon wafer was placed on top of the planetary system at the center of the approximately 11 in diameter deposition chamber. To simplify analysis, rotation for the planetary system was turned off. A deposition of approximately $10.5 \mu\text{m}$ was then carried out using Parylene-C as the dimer. As mentioned in the Thin Channel Experiment section, pressure was able to be logged during the run using a calibrated Pirani gauge near the back of the chamber.

The thickness profile was obtained post-deposition using a Filmetrics F20 white-light interferometer. The operating principles of this tool are similar to those of an ellipsometer in that it fits an interference model based on the film properties to determine the thickness. However, unlike the ellipsometer, the white-light interferometer is only capable of measuring the phase shift Δ of the light. The thickness is then obtained by adjusting model parameters to maximize the goodness of fit of the plot [27]. Using this tool, a map of the wafer was generated automatically using a built-in translation stage.

RESULTS

Thin Channel Experimental Results

A plot of the pressure profile measured in the thin channel gap experiment is shown in figure 8. The initial decrease in pressure is due to the pump-down of the system before the monomer is introduced. Accounting for this, the pressure used for the model was started at the time where the minimum pressure occurred. This minimum pressure is mostly due to residual background gas present in the chamber. Therefore, since the deposition rate depends only on the partial pressure of p-xylylene present, this pressure was subtracted from the result.

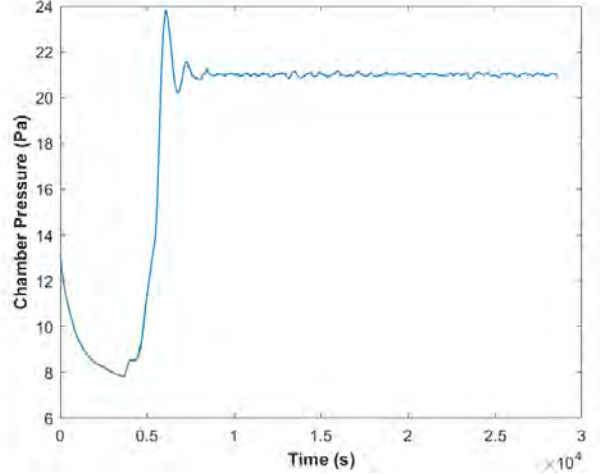


FIG. 8: A plot of the pressure logged by a Pirani gauge during the narrow channel experiment.

In line with Fortin's original Langmuir adsorption model, a value of $m = 1$ was initially chosen for the order of the reaction in the model (5) and (6). However, this was found to fit the data rather poorly when using the externally measured film thickness of $\bar{H} = 8.129 \mu\text{m}$ as the final deposition height. In addition to this, the best fit involved a rather large value of $B = 442.8$ which is difficult to rectify with the known parameters for Parylene. At this value of B , the predicted temperature of the monomer gas is expected to be on the order of 10^{-3} K, which clearly violates the original assumptions in the chamber model.

It was hypothesized that this discrepancy could be the result of the sample receiving a lower pressure of Parylene than was received by the nearby witness used to estimate \bar{H} . This would have resulted in a lower thickness at the gap entrance than expected. Thus, as a second attempt \bar{H} was adjusted to accommodate for this possibility. This did, however, mean that both dimensionless free variables B and $\frac{\bar{H}}{H}$ of the system were allowed to vary which was not ideal for predicting the final deposition properties. A value of \bar{H} equal to one fourth of its original value was found to give a more reasonable fit compared to the original thickness. This can be seen in figure 9. The optimal value of B obtained in this case was also much lower, at a value of 79.01. However, this still gave a physically unreasonable predicted temperature of 0.0032 K.

To deal with this issue, higher values of m were also investigated while maintaining the original the deposition height \bar{H} . A value of $m = 2$, as proposed by Cariou *et al.*, was found to give a better fit as can be seen in figure 9 while also giving a lower value of $B = 293.2$, resulting in a predicted temperature of 0.0037 K [9]. Higher values of m were generally found to give a better fit to

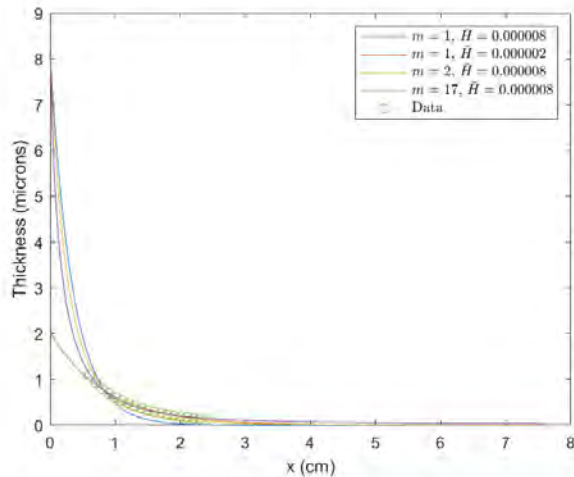


FIG. 9: Plots of fits from the narrow channel experiment at various different values of m and \bar{H} . Values of B were determined by minimizing the RSE error.

TABLE I: Narrow Channel Fit Parameters

m	\bar{H} (μm)	B	T (K)	RSE (μm^2)
1	8.129	441.2	0.002	0.617
1	2.032	314.9	0.0032	0.014
2	8.129	290.2	0.0037	0.146
17	8.129	51.2	0.1994	0.008

the data while also lowering the values of B . Using a value of $m = 17$, as was done in the original paper by Ramachandran *et al.*, gave the best results compared to the lower values of m [7]. Higher values of m could not be thoroughly investigated due to the higher condition numbers of the Jacobian used to solve the spacial problem. At this value of m , the best fit for B was 39.95, giving a still rather unrealistic value of 0.1994 K for the predicted temperature of the gas.

Sticking Coefficient Data

Information on the sticking coefficient of p-xylylene under the steady-state conditions of the current deposition system was obtained using thickness data from the in-situ white-light interferometer active during the narrow channel experiment. Since the pressure during the deposition was kept at a steady value during the run and the time of the initial transience was short compared to the steady-state, the thickness is assumed to grow at a constant rate as predicted by (5). Thus, a linear relationship between thickness and time is expected in the steady-state region. This linear relationship can be seen in 10, which shows values of thickness measured during

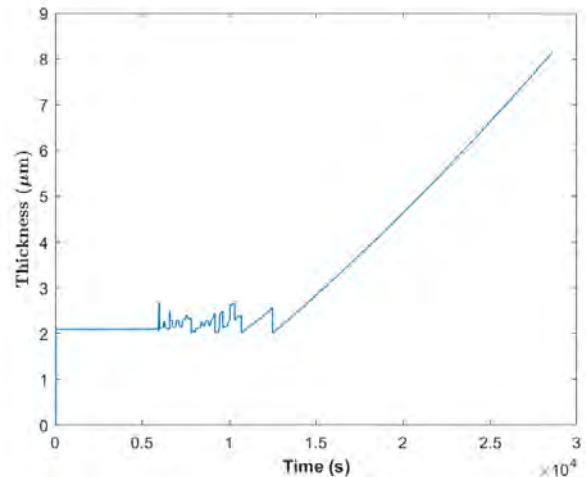


FIG. 10: A plot of the thickness measured on a central witness during the narrow channel experiment using an in-situ white-light interferometer.

the experiment. To quantify the exact degree of linearity, the Pearson correlation coefficient was used to compare between time and thickness data [28]. This coefficient is given in terms of the sample covariance and standard deviations of two random variables x and y as given by,

$$r_{xy} = \frac{\text{cov}(x, y)}{\sigma_x \sigma_y} \quad (36)$$

This value was found to be 0.99883, indicating a high degree of linearity as expected. Thus, it was considered justified to estimate the sticking coefficient assuming a constant growth rate and pressure in equation (1). The value of p in this equation was obtained by averaging the pressure over the steady-state region $t \in [t_0, t_e]$, and the average rate of growth R_d was estimated by using the thickness values d measured at the endpoints of steady-state region:

$$R_d \approx \frac{d(t_e) - d(t_0)}{t_e - t_0}$$

The sticking coefficient could then be obtained by

$$S = \frac{\sqrt{2\pi m k T} R_d}{N_A V_m p} \quad (37)$$

Based on considerations from the previous section that B was generally high, a value of the smallest physically reasonable temperature of the gas was assumed. This temperature would be around room temperature at $T = 293$ K. The molecular volume V_m was estimated using the density of the film as $V_m = \frac{m}{\rho}$, where m is the mass of a single p-xylylene molecule.

Using this value for S , the coverage for the steady-state condition of our deposition system could then be

estimated from equation (2) as

$$(1 - \theta) = S \left(1 + V e^{-\Delta E/kT_s} \right)$$

where the substrate was also assumed to be room temperature. Values of V and ΔE were obtained based on experimental values from Fortin *et al.* as $V = 1.2 \times 10^8$ and $\Delta E = 39.4$ kJ/mol respectively [3]. Performing this calculation, a coverage of $(1 - \theta) = 0.00165$ was obtained. This is close to the value of 0.00129 originally obtained by Fortin in his experiment.

Comparisons of Chamber Thickness Profiles

Using the value of $(1 - \theta)$ obtained in the previous section, the slip boundary conditions were implemented in OpenFOAM. To get the appropriate pressures expected at the pressure gauge, the inlet pressure was iteratively adjusted until the average steady-state pressure at this position was equal to the mean pressure recorded during the experiment, $p_{avg} = 2.7973$ Pa.

115 points uniformly distributed across the surface of the 8-in diameter wafer were used to map the thickness distribution with a white-light interferometer. Measurements were taken across a range 700-1000 nm, and a Cauchy model was used for the index of refraction, n , and extinction coefficient, k , used to fit the measured spectrum.

A plot of the final thickness profile measured is shown in figure 13a, and the pressure recorded during the run is shown in figure 11. Ignoring the initial transience, the pressure was maintained at a steady pressure which justifies the use of steady-state conditions used during the simulation. This also implies a constant growth rate R_d so that the final thickness at any given point \mathbf{x} on the wafer is given by

$$\begin{aligned} d(\mathbf{x}) &= R_d(\mathbf{x})\tau = \frac{N_A V_m S p(\mathbf{x})}{\sqrt{2\pi m k T(\mathbf{x})}} \tau \\ &= \frac{N_A V_m \tau (1 - \theta)}{\sqrt{2\pi m k} (1 + V e^{-\Delta E/RT_s})} \frac{p(\mathbf{x})}{\sqrt{T(\mathbf{x})}} \end{aligned} \quad (38)$$

where τ is the deposition time and the temperature of the substrate, T_s , is room temperature as stated by our boundary conditions.

In order to match pressures obtained on the simulation mesh to points measured on our wafer, a mean value coordinates interpolation scheme was used to map values at the vertices of the mesh to the desired points from the measurement data [29].

Plots showing the pressure and temperature profiles obtained during the simulation are shown in figures 13b and 12. A theoretical thickness profile was then generated from this data using equation (38). To quantify

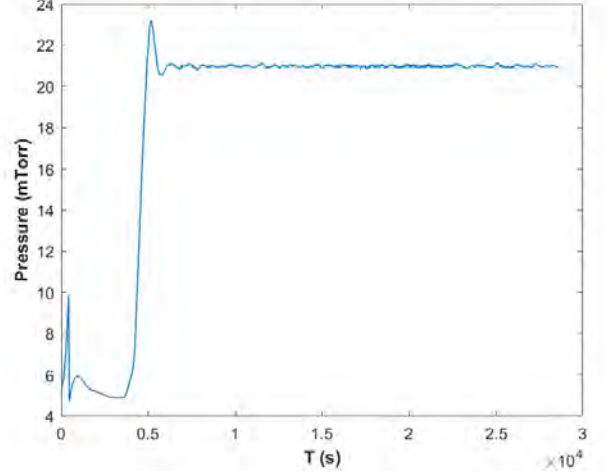


FIG. 11: Pressure data log recorded during simulation experiment.

the error between the current model and experiment, the residual sum of squares was calculated:

$$RSS = \sum_{i=1}^n (d_i^E - d_i^S)^2$$

where d^E and d^S are the experimental and simulated film thicknesses obtained at a point i . Using this method a rather large value of 1.91×10^{-3} μm was obtained. A comparison between figures 13a and 11 reveals this somewhat large discrepancy between predicted and measured thicknesses. Here, a much larger average thickness was predicted than was actually observed. This cannot be explained by the difference in the pressure at the substrate surface and the gauge pressure used for calculating sticking coefficient in equation (37), as the simulation predicts a slightly lower average pressure of 2.6994 Pa than the pressure gauge.

To get around this issue, the value of the deposition coefficient R_D from equation (4) was kept general when analyzing the deposited thicknesses. Noting the linear dependence between d and $\frac{p}{T}$ in equation (38), the predicted thickness can be expressed in the form

$$d(\mathbf{x}) = A (p(\mathbf{x}))^m \quad (39)$$

where A is an arbitrary coefficient and m is the order of the reaction. The accuracy of this model can then be measured by quantifying the degree of correlation between these variables. This all, of course, assumes that temperatures are uniform enough to play a negligible role in variations in the deposition rate across the wafer. This is confirmed by simulation which shows extremely small variations in temperature ranging from only 314.28-314.51 K across the wafer's surface. This method also has the advantage of allowing for the testing of potential

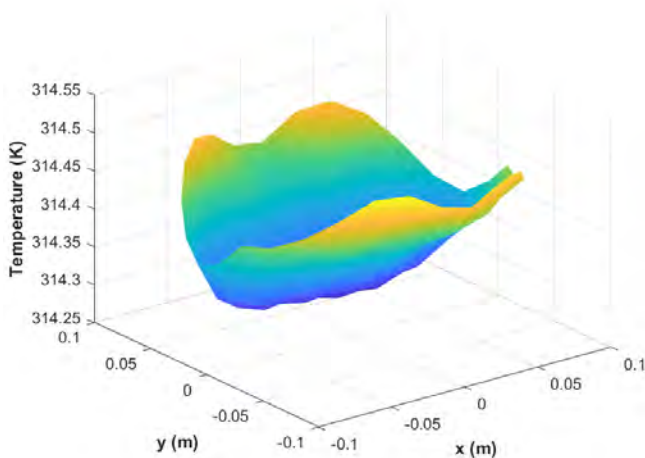


FIG. 12: Simulated temperature profile on an 8 in wafer.

higher order reactions that may occur on the substrate's surface by using the generalized power term m . The correlation between simulated pressure and measured thicknesses was determined using Pearson's correlation coefficient from equation (36).

Using the linear model ($m = 1$), a rather low correlation coefficient of 0.4856 was obtained. Testing the second order ($m = 2$) and $m = 17$ reactions examined during the gap experiment gave slightly higher correlation values of $r = 0.4964$ and $r = 0.4997$ respectively, however, resulting values were still quite low. Finally, the optimal value of m was determined by minimizing the residual sum of squares error using the Nelder-Mead optimization algorithm introduced earlier. For each value of m , the value of A in equation (39) was determined using a linear least-squares fit with a zero y-intercept [28]. In this way, an optimal value of $m = 2.0847$ was obtained. The mean percentage error across the surface of wafer at this value of m was found to be very low at only 0.3276 percent. A plot of this error along the wafer is shown in figure 14.

DISCUSSION

The thin channel results reveal that generally much higher values of the dimensionless parameter B were needed to fit the data than was physically realistic. All values of B obtained in this experiment were found to predict extremely small gas temperatures for reasonable values of the other parameters. Although these other parameters may also vary by small amounts from what was used in this paper (for example ρ may vary from anywhere between 1.153 kg/m^3 and 1.177 kg/m^3 depending on the crystallinity of the deposited Parylene) the main

bulk of this difference could not be accounted for by such small variations alone [1]. A better fit could be obtained by using lower values of film thickness \bar{H} while also improving on the value of B . Even so, the values of B were still high enough that temperatures still did not match with what was expected. The best results could be obtained by increasing the order of the reaction, m . This allowed better fits to be obtained without conflicting with measured values of \bar{H} while also decreasing values of B . However, the values of m needed for these results were found to be so large as to elude any models that have been put forth so far. Similar observations were made by Ramachandran *et al* who originally tried this method and found that a value of $m = 17$ gave the best fit. Although this could reveal a failure of the diffusive model to accurately predict the gas's dynamics, the fact that some physically realistic thickness profiles could be generated more likely indicates that the exact dynamics of Parylene deposition onto surfaces at low pressures is instead the limiting factor.

On the other hand, the p-xylylene flow simulation produced much better consistency between expected pressure profiles and measured film thicknesses. The model correctly predicts higher pressures to be present near the back end of the distribution tube and towards the end of the chamber with the outlet. However, one inconsistency with the model is that higher film thicknesses are expected nearer to the center of the wafer than was simulated. The expected thickness profile across the wafer is expected to resemble that of a saddle. Meanwhile, simulation results do not predict this saddle profile at all, instead giving a uniform thickness profile perpendicular to the axis formed by the distribution tube and outlet. This could potentially indicate that the exact dynamics of the flow near the walls of the chamber isn't being fully accounted for. Given the small variations in temperature present, this would most likely seem to indicate errors in the wall boundary conditions used. From the low values of surface coverage generally reported of p-xylylene, the Langmuir adsorption boundary condition (14) seems to predict a low velocity jump along walls nearing the no-slip condition. It's possible that a more intermediate slip value could more accurately predict the pressures along the outer edge of the wafer while also giving a less uniform temperature profile than what was simulated. However, such a large increase in slip seems unlikely to be rectifiable with the simple adsorption model being considered. Thus, further investigations are still needed into modeling the flow boundary conditions of p-xylylene near walls.

Taking into account the consumption of Parylene into the fluid models could also better explain the lower pressures that were observed near chamber walls. Although these effects were initially neglected due to the low deposition rates of Parylene, these results indicate that gas densities in the chamber could be sufficiently low

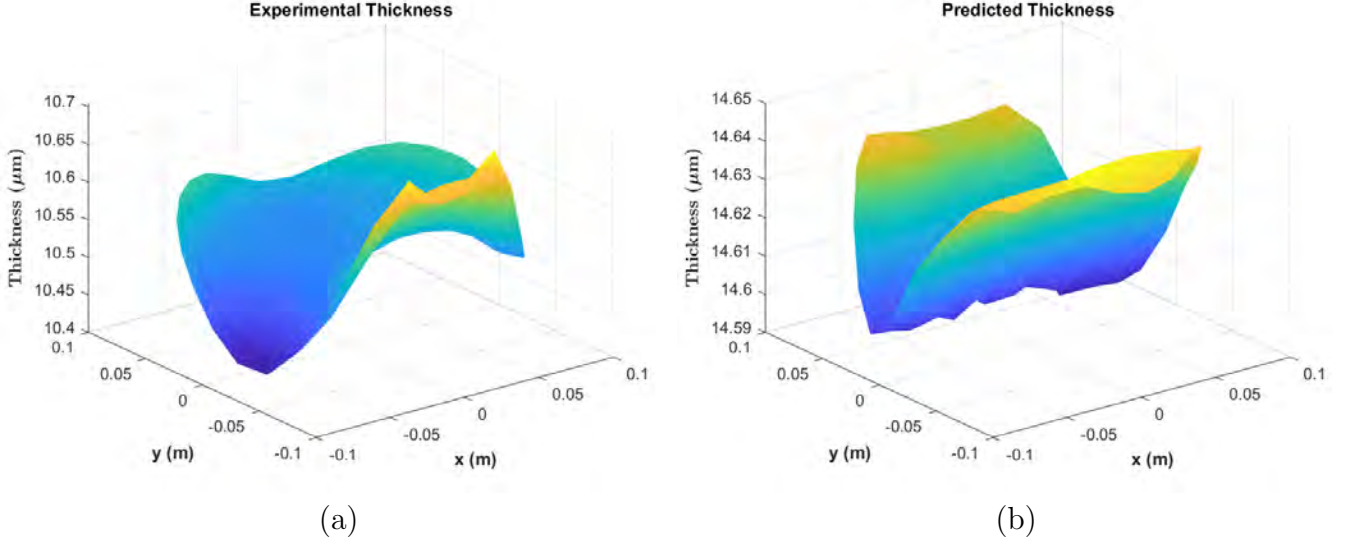


FIG. 13: (a) Experimentally measured thickness profile on an 8 in silicon wafer. (b) Predicted thickness profile from simulations using the calculated value of the sticking coefficient and $m = 1$.

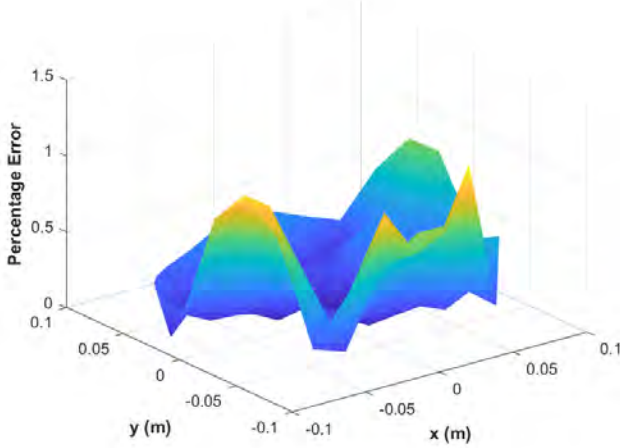


FIG. 14: Profile showing the percent error between measured and simulated thicknesses with $m = 2.0847$.

enough for these effects to become significant. The highly uniform temperature profile also seems to be unrealistic given the difference between wall and inlet gas temperatures, so accounting for thermal effects at the wall surfaces may also be an important effect to simulate.

Although not considered here, future simulations will also need to account for the effects of moving surfaces on gas dynamics so that the uniformity of parts on the rotating planetary system may be considered. This should be a straightforward process as many expressions used here are readily applicable to non-stationary surfaces. For example, slip boundary conditions (14) near moving walls

can be accounted for by setting an appropriate non-zero value of \mathbf{u}_w based on the wall velocity. Additionally, new solvers, such as OpenFOAM's rhoPimpleFoam, may be employed to solve for the N-S-F equations in rotating reference frames, allowing for the use of dynamic meshes which could be used to simulate the motion of the planetary system. Other approaches could include determining the steady-state flow at various sampled rotation positions and extrapolating the final thickness from that. This would be possible since the timescales at which the planetary system moves are expected to be much larger than the timescales at which steady state is reached (which was found to be on the order of milliseconds based on simulation results). As for the deposition rate of Parylene, the kinematics near the surface are not expected to be significantly impacted at such low surface velocities (~ 0.1 m/s at its greatest compared to a flow rate of 45 m/s at the inlet), so this effect would not need to be taken into account.

Overall, the simulation results obtained in this paper reveal that first order models used to describe the reaction rate may not accurately describe the adsorption process of p-xylylene at sufficiently low pressures. Instead, results seem to be more closely aligned with the original second order model predicted for volume phase reactions in Cariou *et al.* [9]. Using Beach's model, this could also indicate that the bulk-phase initiation reaction is of the fifth order. Although this is plausible, it seems unlikely that reactions involving such large amounts of molecules would occur at low pressures and be reduced at higher pressures. However, because thermal effects on film growth weren't able to be fully investigated in this simulation, it is clear that more work is still needed to

understand the kinematics that occur near the surface. Inconsistencies between our own values of m reported between the thin channel experiment and simulation also hints towards a more complex interaction occurring at the film surface. Perhaps surface migration effects, which traditionally aren't accounted for in the rate equation derivations, could explain the failure of these models to accurately predict film growth.

Despite the challenges with modeling the deposition of Parylene, its success in predicting some key features of the flow holds promising for future studies. A model that accounts for some or all of the additional features outlined in this section seems likely to provide better results that more accurately predict the thickness profiles of deposited Parylene films. Future work should involve accounting for these factors as well as future investigations into the exact kinematic and chemical processes that occur near surface boundaries at low pressures.

CONCLUSION

Using a rarefied fluid model to simulate the deposition of p-xylylene combined with the best current correlation functions for its fluid properties, an accurate model of Parylene film growth was able to be obtained that successfully predicts key features of the pressure profile. Despite this, results still show some potential inconsistencies in the gas flow near the walls of the chamber. This indicates that exact values of the coefficients used in the velocity slip and temperature jump boundary conditions may be inaccurate, or that a potentially new model for these boundary conditions is needed altogether. Similarly, deposition rate results from both the narrow channel and simulation experiments reveal that the adsorption of Parylene at low pressures is still a relatively poorly understood phenomenon. The overall discrepancies between these experiments and reality were difficult to rectify in addition to being inconsistent among themselves, indicating that there is still much to be learned about the inner workings of these processes. Although fairly accurate models were eventually able to be obtained in both cases, these results were inconsistent and lacked theoretical justification.

Further research is still needed to elucidate the processes that occur near boundary surfaces during Parylene CVD. This includes a more advanced consideration of the various kinematic phenomena affecting the bulk flow of the fluid, as well as the thermodynamic and chemical processes which determine the deposition properties. Despite these difficulties, deposition profiles from the simulation were fairly accurate in predicting key flow features resulting in deposition. Potentially opening the door towards future applications in modeling some industrial and commercial processes. However, a more detailed description of the deposition process is still needed for any

applications where a high degree accuracy is desired, motivating the need for further studies of this material in the future.

ACKNOWLEDGMENTS

Huge thanks goes out to my project advisor, Dr. Steven Larson, for his continued support of this research project over the past year, as well as Sandia National Laboratories for allowing me to work on this project in collaboration with the University of New Mexico. I would also like to acknowledge Alex Mings for his guidance and support in teaching me how to run the deposition systems used in this paper. This project would not have been possible without the time, tools, and resources afforded to me at Sandia, and I am extremely thankful for the opportunity to work on such an involved and detailed research project as a part of my Senior thesis.

REFERENCES

-
- [1] M. Gazicki, G. Surendran, W. James, and H. Yasuda, Polymerization of para-xylylene derivatives (parylene polymerization). iii. heat effects during deposition of parylene n at different temperatures, *Journal of Polymer Science Part A: Polymer Chemistry* **24**, 215 (1986).
 - [2] M. Szwarc, Some remarks on the ch2[graphic omitted]ch2 molecule, *Discuss. Faraday Soc.* **2**, 46 (1947).
 - [3] J. B. Fortin and T.-M. Lu, A model for the chemical vapor deposition of poly(para-xylylene) (parylene) thin films, *Chemistry of Materials* **14**, 1945 (2002), <https://doi.org/10.1021/cm010454a>.
 - [4] W. F. Gorham, A new, general synthetic method for the preparation of linear poly-p-xylylenes, *Journal of Polymer Science Part A-1: Polymer Chemistry* **4**, 3027 (1966).
 - [5] S. F. Bröskamp, D. Redka, A. Möhlmann, G. Franz, and D. Jocham, Chemical vapor deposition of poly-p-xylylene in narrow tubes, *AIP Advances* **7**, 075005 (2017).
 - [6] I. Langmuir, The adsorption of gases on plane surfaces of glass, mica and platinum., *Journal of the American Chemical Society* **40**, 1361 (1918), <https://doi.org/10.1021/ja02242a004>.
 - [7] A. Ramachandran, M. Junk, K. P. Koch, and K.-P. Hoffmann, A study of parylene c polymer deposition inside microscale gaps, *IEEE Transactions on Advanced Packaging* **30**, 712 (2007).
 - [8] L. Asnin, Y. Chekryshkin, and A. Fedorov, Calculation of the sticking coefficient in the case of the linear adsorption isotherm, *Russian Chemical Bulletin - RUSS CHEM BULL* **52**, 2747 (2003).
 - [9] F. Cariou, D. Valley, and W. Loeb, Poly-para-xylylene in thin film applications, *IEEE Transactions on Parts, Materials and Packaging* **1**, 54 (1965).

- [10] J. B. Fortin and T.-M. Lu, *Chemical vapor deposition polymerization: The growth and properties of parylene thin films*, 2004th ed. (Kluwer, 2003).
- [11] W. F. Beach, A model for the vapor deposition polymerization of p-xylylene, *Macromolecules* **11**, 72 (1978).
- [12] B. Guo and B. Xie, On the dynamics of navier-stokes-fourier equations (2017), arXiv:1712.02510 [math.AP].
- [13] J. C. Maxwell, Vii. on stresses in rarified gases arising from inequalities of temperature, *Philosophical Transactions of the Royal Society of London* **170**, 231 (1879).
- [14] A. Gavasane, S. Sachdev, B. Mittal, U. Bhandarkar, and A. Agrawal, A critical assessment of the maxwell slip boundary condition for rarified wall bounded flows, *International Journal of Micro-Nano Scale Transport* **2**, 109 (2011).
- [15] S. Colin, Gas Microflows in the Slip Flow Regime: A Critical Review on Convective Heat Transfer, *Journal of Heat Transfer* **134**, 020908 (2011).
- [16] N. Le, C. White, J. Reese, and R. Myong, Langmuir-maxwell and langmuir-smoluchowski boundary conditions for thermal gas flow simulations in hypersonic aerodynamics, *International journal of heat and mass transfer* **55**, 5032 (2012).
- [17] Y. Zhou, J. Wu, and E. W. Lemmon, Thermodynamic Properties of o-Xylene, m-Xylene, p-Xylene, and Ethylbenzene, *Journal of Physical and Chemical Reference Data* **41**, 023103 (2012), https://pubs.aip.org/aip/jpr/article-pdf/41/2/023103/15726138/023103.1_online.pdf.
- [18] E. W. Lemmon, M. O. McLinden, and W. Wagner, Thermodynamic properties of propane. iii. a reference equation of state for temperatures from the melting line to 650 k and pressures up to 1000 mpa, *Journal of Chemical & Engineering Data* **54**, 3141 (2009).
- [19] S. K. Mylona, K. D. Antoniadis, M. J. Assael, M. L. Huber, and R. A. Perkins, Reference Correlations of the Thermal Conductivity of o-Xylene, m-Xylene, p-Xylene, and Ethylbenzene from the Triple Point to 700 K and Moderate Pressures, *Journal of Physical and Chemical Reference Data* **43**, 043104 (2014).
- [20] B. Balogun, N. Riesco, and V. Vesovic, Reference Correlation of the Viscosity of para-Xylene from the Triple Point to 673 K and up to 110 MPa, *Journal of Physical and Chemical Reference Data* **44**, 013103 (2015).
- [21] N. Dongari, A. Sharma, and F. Durst, Pressure-driven diffusive gas flows in micro-channels: from the knudsen to the continuum regimes, *Microfluidics and Nanofluidics* **6**, 679 (2009).
- [22] D. V. Schroeder, *An introduction to thermal physics*, 1st ed. (Addison Wesley Longman, 2005).
- [23] J. Hales and R. Townsend, Liquid densities from 293 to 490 k of nine aromatic hydrocarbons, *The Journal of Chemical Thermodynamics* **4**, 763 (1972).
- [24] S. Hamdi, W. E. Schiesser, and G. W. Griffiths, Method of lines, *Scholarpedia* **2**, 2859 (2007), revision #124335.
- [25] Introduction to spectroscopic ellipsometry, in *Spectroscopic Ellipsometry* (John Wiley & Sons, Ltd, 2007) Chap. 1, pp. 1–11.
- [26] J. C. Lagarias, J. A. Reeds, M. H. Wright, and P. E. Wright, Convergence properties of the nelder–mead simplex method in low dimensions, *SIAM Journal on Optimization* **9**, 112 (1998), <https://doi.org/10.1137/S1052623496303470>.
- [27] *Operations Manual for the Filmetrics F20*, Filmetrics, Inc., revision 7.3.2.0 ed. (2013).
- [28] J. R. Taylor, *An Introduction to Error Analysis: The Study of Uncertainties in Physical Measurements*, 2nd ed. (University Science Books, 1997).
- [29] T. Ju, S. Schaefer, and J. Warren, Mean value coordinates for closed triangular meshes, *ACM Transactions on Graphics* , 561 (2005).